

Sequential Crystallization of Pyrrhotite, Cubanite, and Intermediate Solid Solution from Cu–Fe–(Ni)–S Melt¹

E.F. Sinyakova^{a, ✉}, V.I. Kosyakov^b, K.A. Kokh^{a,c}, E.A. Naumov^{a,c}

^a V.S. Sobolev Institute of Geology and Mineralogy, Siberian Branch of the Russian Academy of Sciences, pr. Akademika Koptyuga 3, Novosibirsk, 630090, Russia

^b A.V. Nikolaev Institute of Inorganic Chemistry, Siberian Branch of the Russian Academy of Sciences, pr. Akademika Lavrent'eva 3, Novosibirsk, 630090, Russia

^c Novosibirsk State University, ul. Pirogova 2, Novosibirsk, 630090, Russia

Received 15 August 2018; received in revised form 18 October 2018; accepted 8 November 2018

Abstract—We present the results of quasi-equilibrium directional crystallization of melt of the composition (mol.%): Fe = 31.9, Ni = 1.7, Cu = 16.0, S = 50.4. The produced ingot consisted of the following zones: monosulfide solid solution *mss* + isocubanite *icb* (CuFe₂S₃) + Cu₃Fe₄S₇ // *icb* + intermediate solid solution *iss* (~Cu₂Fe₃S₅) + pentlandite // mixture of unidentified decay products of solid solution *iss*₁ // chalcopyrite *cp* + putoranite *put* // *cp* + talnakhite *tal* + bornite *bn*. The results of chemical analysis of the ingot were used to construct the distribution curves of the components in the solid and to calculate the change in the composition of sulfide melt (*L*) during directional crystallization in four zones of the ingot. Phase reactions involving a melt have been established. It is shown that the Cu–Fe–Ni–S system has a two-phase equilibrium region *L* + *icb**. A similar region was earlier found in the ternary Cu–Fe–S system. A crystallization zone of two intermediate solid solutions *iss*₁ and *iss*₂, which were earlier obtained by the common method of isothermal annealing and quenching, has been revealed. The peritectic character of crystallization of the phases *icb**, *iss*₁, and *iss*₂ from the melt is established. The results obtained show the fundamental possibility of the existence of a new type of zoning in the formation of copper-nickel low-sulfur sulfide orebodies.

Keywords: system Cu–Fe–(Ni)–S, phase equilibria, zoning, fractional crystallization

INTRODUCTION

The formation of zoned massive ores from the copper-nickel Noril'sk deposit is most frequently attributed to the fractionation crystallization of a multicomponent sulfide melt in exo- and endocontacts of layered intrusions, though a generally accepted description of this process is still unavailable (Kosyakov et al., 2012). In this case, the ore body is separated into several zones, which are arranged regularly relative to each other. Each zone is formed from a particular mineral paragenesis. Inside the zones, the proportions of minerals, their chemical compositions and respective local (averaged over characteristic volume) chemical compositions of paragenesis can change gradually. Transition from one zone to the other leads to the appearance and disappearance of some minerals, i.e., results in a new paragenesis. The average chemical composition of the solid body at the boundary between the zones changes abruptly. Zoned samples, which are similar in structure to the ore bodies of magmatogenic copper-nickel deposits, can be obtained in

laboratory experiments on directed crystallization of multi-component melts that simulate the compositions of natural sulfide melts. The relationship between the regularities of the formation of directional crystallized samples and the structure of the melting diagrams of ternary systems are considered in (Kosyakov and Sinyakova, 2012).

Magmatic sulfide liquid consists of a large number of geochemically significant components, but to analyze the formation of major ore-forming minerals at copper-nickel deposits, it is sufficient in the first approximation to study the processes taking place in the Cu–Fe–Ni–S system.

During the formation of ore bodies, crystallization conditions are close to quasi-equilibrium. In this case, the diffusion in crystalline phases is negligible, the melt has a homogeneous composition and thermodynamic equilibrium is retained at the crystallization front. It is convenient to use the fraction of solidified melt *g* as the coordinate of the process. The concentration of the *i*th component in the initial melt *c*₀^{*i*} in the current melt *c*_{*L*}^{*i*} and in the solid at the crystallization front *c*_{*S*}^{*i*} are related by the expression

$$c_L^i = \frac{c_0^i - \int_0^g c_S^i(g) dg}{1 - g}. \quad (1)$$

¹This paper was translated by the authors.

✉ Corresponding author.

E-mail address: efsin@igm.nsc.ru (E.F. Sinyakova)

Here $i = \text{Cu, Fe, Ni, S}$. Eq. (1) is the result of the material balance equation of the i th component. In the zoned ore body, the functions $c_L^i(g)$ is a smooth curve. The j th break point at g_j^* corresponds to the boundary between the j th and $(j + 1)$ th zones. The function $c_S^i(g)$ undergoes a discontinuity at this point.

To apply equation (1) to real ores, it is necessary to suggest the acceptability of the above-mentioned assumptions and have a 3D tomographic map of the distribution of components in the volume of the ore body. Data (1) can be used for the creation of the trajectory $F_L(c_L^1, c_L^2, c_L^3) = f(g)$ in the 3D concentration tetrahedron and 2D projections on the faces. This piecewise smooth curve is oriented toward decreasing temperature. Its j th segment corresponds to the crystallization of the j th zone. In a quaternary system, from one to four phases can crystallize from the melt, which are solid solutions or stoichiometric compounds. Therefore, each curvilinear segment of melt-composition trajectory can be compared with the corresponding segment of solid-phase composition on single-phase crystallization or average composition of the ingot on multiphase crystallization. The set of these segments describes the crystallization path inside the concentration tetrahedron. The relationships between the composition of melt and each of the solid phases during crystallization is depicted in the form of conode fans. Thus, it is convenient to depict the relationship between the melt composition and average composition of solid ingot at a specific value of g (Kosyakov and Sinyakova, 2017a). Equations (1) are applicable to the ore body, if we assume that crystallization takes place in a quasi-equilibrium mode, the phase diagram of the Cu–Fe–Ni–S system is known in detail and the topographic maps of distribution of components in the ore body volume have been built. However, such calculations have not been carried out so far.

The analogy between the fractionation crystallization of an ore body with a complicated shape and the directed crystallization of a cylindrical sample provides an opportunity for modeling the regularities of formation of zoned ore bodies in laboratory conditions. In this experiment, a cylindrical ingot with a particular sequence of zones is formed.

Results of the study of this ingot allow us to construct curves $c_L^i(g)$ и $c_S^i(g)$, and the additional data on the phases from different sections of the sample make it possible to interpret crystallization processes of primary phases from the melt as well as the complete or partial decomposition of primary phases on further cooling. It is worth noting that the trajectory of the melt is uniquely determined by the structure of the solid-liquid diagram and the composition of the initial melt (Kosyakov and Sinyakova, 2012). Therefore, each point of the melt's composition is a source for a single trajectory with a z_q zonality, which is determined by the crystallization sequence of primary phases in the zones of crystallized samples. At the end of crystallization, the compositions of the melt and the solid body are identical. A great number of melt compositions from which samples with a similar zonality are obtained belong to the 3D region inside

the tetrahedron. The whole concentration tetrahedron is divided into such regions². However, in the study of the features of formation of zoned ore bodies we only focus on that part of the tetrahedron volume which includes the compositions of natural sulfide melts and its division into regions of compositions providing different types of zonality.

Owing to the insufficient research on the phase diagram of the Cu–Fe–Ni–S system and lack of consistent data on the thermodynamic properties of sulfide melt and solid phases, it is impossible to make a reliable a priori prediction of probable types of zonality of ore bodies. Published fragments of the phase diagram of the quaternary system and ternary boundary systems suggest that at the beginning of the process the monosulfide solid solution mss $(\text{Ni}_z(\text{Fe,Cu})_{1-z})\text{S}_{1±δ}$, is the first to crystallize, followed by an intermediate solid solution iss $(\text{Cu}_x\text{Fe}_{1+x})\text{S}_{2-y}$ which, on cooling, decomposes into other minerals. The existence of copper-nickel ores with different chemical and mineral compositions suggests the realization of several types of zonality of ore bodies, but the list of probable types of zonality and genetic schemes of their formation is still absent. Answers to these questions can be obtained from the experiments on the directed crystallization of melts, which simulate different compositions of natural sulfide liquids. Earlier, we carried out experiments on the simulation of the formation of pyrrhotite-cubanite, pentlandite-bornite and other mineral varieties of massive ore bodies from the Noril'sk deposit: (Kosyakov et al., 2012; Kosyakov and Sinyakova, 2014, 2017a,b; Sinyakova and Kosyakov, 2009, 2012; Sinyakova et al., 2016). For example, in (Kosyakov et al., 2012) results of crystallization of two samples with similar compositions are reported: Fe 32.55, Cu 10.70, Ni 5.40, S 51.00, Pt = Pd = Rh = Ru = Ir = Au = Ag = 0.05 mol.% (sample I) and Fe 33.74, Cu 15.94, Ni 1.48, S 48.75, Pt = Pd = 0.05 mol.% (sample II). The primary zonality of these samples is described by the following sequence of primary phases in the zones: monosulfide/intermediate solid solutions. The observed phase composition of samples after cooling corresponds to secondary zonality. Sample I consists of three zones: monoclinic pyrrhotite/mixture of hexagonal pyrrhotite and tetragonal chalcopyrite/mixture of tetragonal and cubic chalcopyrite, pentlandite and bornite, and sample II has four zones: mixture of hexagonal pyrrhotite, cubanite and pentlandite/mixture of low-sulfur pc -phase of haycockite composition described in (Cabri, 1973) and pentlandite/mixture of mooihoeite and bornite. It is apparent that a relatively minor variation in the composition of the initial melt can lead to a sharp change in the zonality of the sample. These results show a more complicated structure of the solid-liquid diagram of the Cu–Fe–Ni–S system compared to those described in literature (e.g., (Craig and Kullerud, 1969; Fleet and Pan, 1994)).

² An example of construction of compositional triangle of the Fe–Ni–S system, divided into zones with different topologies of melt trajectory, is reported in (Kosyakov and Sinyakova, 2012).

To understand the physicochemical features of formation of ore bodies, it is expedient to conduct additional researches on the directed crystallization of melt that simulate sulfide liquids of different compositions. In this work we have described a new type of zonality of a sample on the basis of results of quasi-equilibrium directed crystallization of the following melt (in mol.%): 31.9 Fe, 1.7 Ni, 16.0 Cu, 50.4 S. This composition simulates the compositions of natural sulfide magmatic melts typical of copper-rich and nickel-poor ores from the copper-nickel Noril'sk deposits, with the ratio $S/Ni + Cu = 1.44$, $Ni/Cu = 0.11$ (Czamanske et al., 1992; Naldrett, 2004, 2010).

EXPERIMENTAL PART

The starting sample was prepared from Cu, Fe, Ni (99.99%) and sulfur (99.9999%), additionally purified by vacuum distillation, taken in a predetermined ratio. The directed crystallization of a 20 g sample, which was preliminarily synthesized from a melt, was performed by the Bridgman method by moving the ampoule from the hot zone to the cold zone at a rate of 2.3×10^{-8} m/s (Kosyakov and Sinyakova, 2005). These conditions provided a quasi-equilibrium mode for the process. The temperature in the lower part of the quartz ampoule was 1025 °C at the beginning of crystallization, and 825 °C at the end. After crystallization, the ampoule was cooled in air at an average rate of ~ 100 deg/min.

The obtained ingot ~ 120 mm in length and ~ 8 mm in diameter was cut perpendicular to the longitudinal axis into 19 parts. These fragments were weighed to determine the fraction of crystallized melt g . Seventeen fragments were used to prepare polished sections, which were studied using the procedures of microscopic, chemical and X-ray phase analysis. The measurement of the average chemical composition of the ingot and local composition of the main ore-forming sulfides was carried out by energy-dispersion spectrometry (SEM/EDS) on a high-resolution MIRA 3 LMU microscope (Tescan Orsay Holding), equipped with X-ray microanalysis systems: INCA Energy 450+ X-Max 80 and INCA Wave 500 (Oxford Instruments Nanoanalysis Ltd) (Lavrent'ev et al., 2015). The analysis was performed in the Analytical Center for Multi-Elemental and Isotope Research, SB RAS (analyst N.S. Karmanov). The measurements were carried out at the accelerating voltage 20 kV, probe current 1.5 nA, live acquisition time of spectra 30 s. For the analysis, we used the K-series of X-rays. FeS_2 and pure metals Fe, Cu and Ni were used as reference samples. The minimum detection limit of the determined concentrations of elements was 0.1–0.2 wt.%. To decrease the influence of microrelief of the samples on the accuracy of the analysis, spectra on single-phase grains of no more than 5 μm in size were selected by scanning 10 μm^2 zones. The phases smaller than 5 μm were analyzed by a point probe. The average composition of multiphase zones was estimated using the total spectrum obtained from scanning of 1 mm^2 zones. In this case, to

reduce the lower boundary of determined concentrations by about times, the acquisition time of spectra was increased to 120 s. The accuracy of determining the average composition of multiphase zones is 1–2 rel.%, which was revealed in (Sinyakova et al., 2016) on the example of determination of the average composition of the mixture of pyrrhotite and cubanite. In this work, the average composition of multiphase mixtures was calculated from 3–5 analyses from different parts of each section along the ingot. Standard deviations are reported in Table 1.

RESULTS

The procedure for determining the sequence of separation of primary phases during directed crystallization, on the basis of data on the change in the chemical composition along the ingot, is described in (Kosyakov and Sinyakova, 2010). Table 1 shows the experimental data obtained in this work. The phases separated from the melt were identified using the data of microstructural studies of samples along the ingot cooled to room temperature, despite the complete or partial decomposition of primary phases.

Microscopic description of the sample. The photo of the ingot (Fig. 1a) shows that it consists of five visually distinct zones with different microstructures. This is reflected in the below-given scheme of the ingot (Fig. 1b) and microstructures of each zone (Fig. 1c). The first part of the ingot (about 30 vol.%) is dense, and zones II–V contain surface and internal pores the number of which increases drastically towards the end of the ingot. Data on the phase compositions in the samples are given in Table 1.

Zone I ($0 \leq g \leq 0.3$) occupies the left part of Fig. 1c ($g \sim 0.3$). The average chemical composition of substance in the zone varies from $Fe_{40.54}Ni_{1.89}Cu_{4.38}S_{53.19}$ to $Fe_{39.86}Ni_{2.05}Cu_{5.22}S_{52.87}$ (Table 1). Data on the structure of the phase diagram of the Cu–Fe–Ni–S system (Craig and Kullerud, 1969; Ebel and Naldrett, 1997) indicate that in the concentration tetrahedron there is a three-dimensional region of the primary crystallization of monosulfide solid solutions (*mss*). The average composition of the sample in Zone I corresponds to Fe-rich *mss* with minor Cu and Ni, which were separated directly from the melt. The microstructure of the sample consists of *mss* matrix $Fe_{43.0 \pm 0.2}Ni_{2.3 \pm 0.1}Cu_{1.1 \pm 0.1}S_{53.5 \pm 0.1}$ and lamellar inclusions of nonstoichiometric isocubanite $Cu_{1.1}Fe_{1.9}S_3$ (*icb**)³ from ~ 2 to 70 μm thick and a few mm long (Fig. 2a). At present, we cannot unambiguously determine whether these inclusions are the results of cocrystallization of *mss* and *icb** from melt or partial decomposition of primary *mss* at decreased temperature.

When viewed at high magnification, it is clear that *icb** is a mixture of two phases which most likely the decay products of *icb** on cooling (Fig. 2b). The main phase is *icb*

³ The formation of *icb* and *icb** phases during directional crystallization was observed in (Kosyakov and Sinyakova, 2014, 2017b).

Table 1. Average concentrations of components in solid phases and in the melt and distribution coefficients of components between the phases and the melt

g	Solid phase composition, mol.%				Melt composition, mol.%				κ (solid/L)			
	Fe	Ni	Cu	S	Fe	Ni	Cu	S	Fe	Ni	Cu	S
Zone I <i>mss</i> ($0 \leq g \leq 0.30$)												
0.00	40.54 ± 0.08	1.89 ± 0.01	4.38 ± 0.06	53.19 ± 0.01	32.06	1.71	15.80	50.43	1.26	1.11	0.28	1.05
0.09	40.36 ± 0.21	1.92 ± 0.05	4.66 ± 0.11	53.06 ± 0.01	31.02	1.68	17.19	50.11	1.30	1.14	0.27	1.06
0.14	40.25 ± 0.16	1.93 ± 0.01	4.83 ± 0.02	52.99 ± 0.13	30.41	1.67	18.01	49.92	1.32	1.16	0.27	1.06
0.15	40.23 ± 0.13	1.93 ± 0.04	4.86 ± 0.16	52.98 ± 0.01	30.28	1.66	18.18	49.88	1.33	1.16	0.27	1.06
0.23	40.06 ± 0.08	1.96 ± 0.01	5.12 ± 0.19	52.86 ± 0.08	29.36	1.64	19.38	49.61	1.37	1.20	0.26	1.07
0.30	39.86 ± 0.01	2.05 ± 0.11	5.22 ± 0.11	52.87 ± 0.26	28.51	1.62	20.53	49.34	1.41	1.27	0.25	1.07
Zone II <i>icb*</i> ($0.30 \leq g \leq 0.32$)												
0.32	30.59 ± 0.42	0.86 ± 0.11	17.96 ± 0.16	50.58 ± 0.19	28.27	1.62	20.85	49.26	1.08	0.53	0.86	1.03
Zone III <i>iss₁</i> ($0.32 \leq g \leq 0.87$)												
0.38	27.62 ± 0.19	1.65 ± 0.11	20.90 ± 0.21	49.83 ± 0.15	28.31	1.63	20.91	49.15	0.98	1.01	1.00	1.01
0.46	27.77 ± 0.28	1.63 ± 0.20	20.80 ± 0.33	49.80 ± 0.19	28.42	1.61	20.83	49.13	0.98	1.01	1.00	1.01
0.47	27.80 ± 0.31	1.63 ± 0.16	20.78 ± 0.23	49.80 ± 0.01	28.44	1.61	20.82	49.12	0.98	1.01	1.00	1.01
0.55	27.95 ± 0.22	1.61 ± 0.10	20.68 ± 0.27	49.77 ± 0.08	28.54	1.61	20.84	49.01	0.98	1.00	0.99	1.02
0.62	28.08 ± 0.29	1.59 ± 0.16	20.59 ± 0.21	49.74 ± 0.08	28.62	1.62	20.91	48.84	0.98	0.98	0.98	1.02
0.68	28.20 ± 0.11	1.57 ± 0.11	20.51 ± 0.08	49.72 ± 0.08	28.69	1.64	21.03	48.63	0.98	0.96	0.98	1.02
0.81	28.44 ± 0.11	1.54 ± 0.01	20.34 ± 0.13	49.67 ± 0.11	28.82	1.70	21.43	48.04	0.99	0.92	0.94	1.03
0.87	28.57 ± 0.12	1.52 ± 0.01	20.26 ± 0.11	49.65 ± 0.01	28.88	1.74	21.71	47.67	0.99	0.87	0.93	1.04
Zone IV <i>iss₂</i> ($0.87 \leq g \leq 0.96$)												
0.92	25.44 ± 0.16	1.51 ± 0.05	24.00 ± 0.07	49.04 ± 0.01	30.95	1.91	20.91	46.22	0.82	0.79	1.15	1.06
0.96	25.25 ± 0.15	1.38 ± 0.03	24.32 ± 0.18	49.05 ± 0.08	36.91	2.47	17.35	43.27	0.68	0.56	1.40	1.13

$\text{Fe}_{32.4 \pm 0.6} \text{Cu}_{16.8 \pm 0.5} \text{S}_{50.4 \pm 0.1}$ with 0.4 mol.% Ni. The second phase of composition $\text{Fe}_{28.4 \pm 0.6} \text{Ni}_{0.2} \text{Cu}_{20.9 \pm 0.5} \text{S}_{50.5 \pm 0.1}$ is present in the *icb* matrix as a system of thin oriented lamellas $\leq 1\text{--}2 \mu\text{m}$ wide and to 15 μm long. Its composition corresponds to the formula $\text{Cu}_3(\text{Fe,Ni})_4\text{S}_{7.1}$. The content of Ni is close to minimum detection limit of the electron microprobe.

Zone II ($0.3 \leq g \leq 0.32$) occupies 2 wt.% of the sample. It differs drastically in microstructure and chemical composition from *Zone I* (right part Fig. 1c, $g \sim 0.3$). The average chemical composition $\text{Cu}_{17.7} \text{Fe}_{30.9} \text{Ni}_{0.8} \text{S}_{50.5}$ in the zone (Table 1) can be attributed to nonstoichiometric isocubanite (*icb**) with the idealized formula $\text{Cu}_{1.1} \text{Fe}_{1.9} \text{S}_3$, which crystallizes directly from the melt. We showed that in the Cu–Fe–S system, *icb** (Kosyakov and Sinyakova, 2017b) and stoichiometric isocubanite *icb* (Kosyakov and Sinyakova, 2014) can crystallize from the melt. Hence, these regions of two-phase crystallization must be also present on the solid-liquid diagram of the Cu–Fe–Ni–S system. It can be suggested from Fig. 3 that primary *icb** decomposes completely into three phases on cooling. Two of them are present as a system of oriented lamellas of stoichiometric isocubanite CuFe_2S_3 (*icb*) and intermediate solid solution *iss* of composition $\sim \text{Cu}_2\text{Fe}_3\text{S}_5$. The third phase is present as small grains less than 0.5 μm in size. We did not manage to determine the exact composition of grains but the high content of Ni (~ 8 mol.%) suggests that these are pentlandite inclusions.

Zone III ($0.32 \leq g \leq 0.87$) occupies the larger part of the ingot (Fig. 1b). The average composition varies from $\text{Fe}_{27.62} \text{Ni}_{1.65} \text{Cu}_{20.90} \text{S}_{49.83}$ to $\text{Fe}_{28.57} \text{Ni}_{1.52} \text{Cu}_{20.26} \text{S}_{49.65}$ (Table 1). This solution can be referred to the Ni-bearing intermediate solid solution *iss₁* described in (Fleet and Pan, 1994). The microstructure of the sample in the zone consists of unidentified alternating plates of gray and dark gray colors of about 1 μm in width and light gray small inclusions with dimensions of up to $2 \times 2 \mu\text{m}^2$ (Fig. 1c, $g = 0.81$). It was impossible to determine the exact composition of the inclusions. Analysis of the largest grains showed the presence of up to ~ 18 mol.% Ni and lower sulfur content (about 48 mol.%) compared to the surrounding matrix, which suggests that this phase is pentlandite.

Zone IV ($0.87 \leq g \leq 0.96$). The average composition $\text{Fe}_{25.35} \text{Ni}_{1.45} \text{Cu}_{24.16} \text{S}_{49.04}$ in the zone corresponds to *iss₂* (Table 1). An intermediate solid solution of similar composition was described in (Fleet and Pan, 1994). The sample is the decay structure of this phase in the form of alternating plates of Ni-bearing chalcopyrite ($\text{Fe}_{24.1} \text{Ni}_{0.8} \text{Cu}_{24.6} \text{S}_{49.9}$, *cp*) and, most likely, Ni-enriched putranite ($\text{Fe}_{24.8} \text{Ni}_{1.9} \text{Cu}_{24.2} \text{S}_{49.1}$, *put*) (Fig. 1c, $g = 0.96$).

Zone V ($0.96 \leq g \leq \sim 1$) occupies a small volume at the end of the ingot. The average composition in the zone is described by the formula $\text{Fe}_{23.6} \text{Ni}_{2.0} \text{Cu}_{26.2} \text{S}_{48.2}$. It is worth noting that the *iss* solid solution of similar composition was

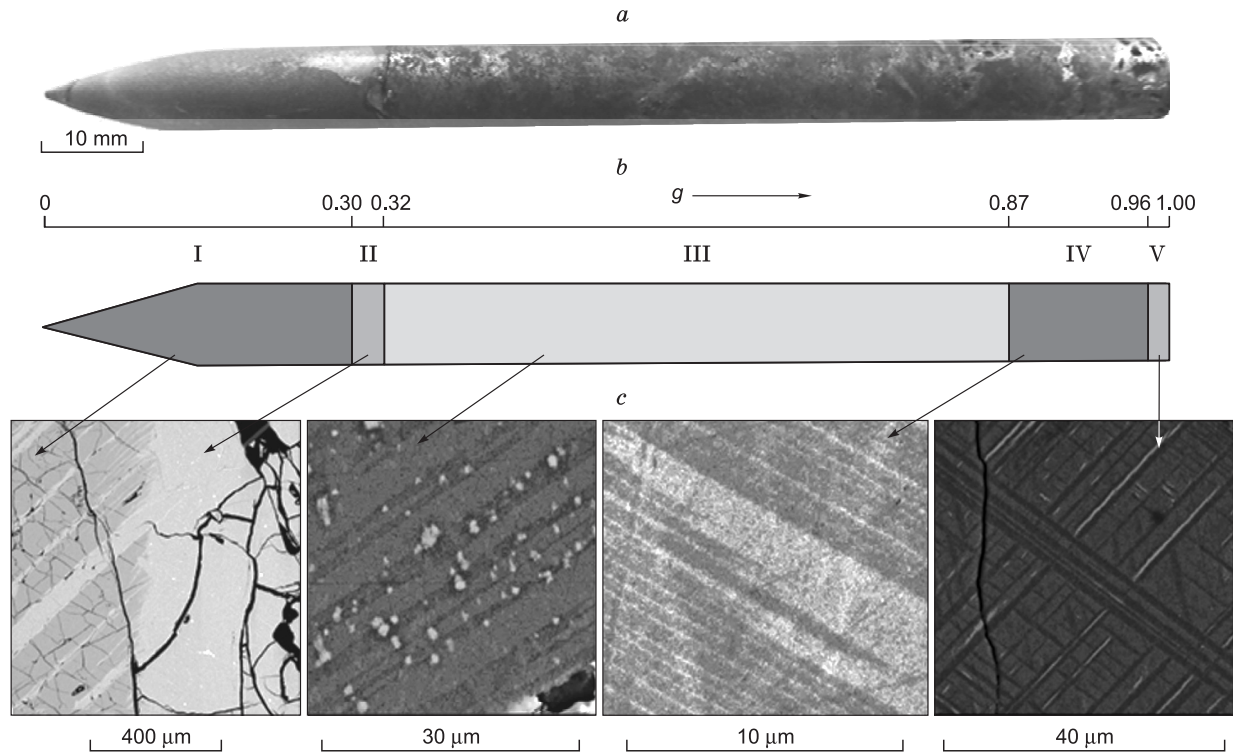


Fig. 1. Photograph in reflected light of directly crystallized sample (a), scheme of zonality (b) and photomicrographs, made in back-scattered electrons, of zones (c) at $g \sim 0.30$ (I/II), 0.32 (II), 0.81 (III), 0.96 (IV), ~ 1 (V). See the text for comments.

found in (Fleet and Pan, 1994). Its decay products on cooling are bornite $\text{Fe}_{14.5}\text{Ni}_{0.2}\text{Cu}_{42.2}\text{S}_{43.1}$ (*bn*) (Fig. 1c, $g \sim 1$, light gray plates) and two phases of similar composition, probably, talnakhite $\text{Fe}_{24.1}\text{Ni}_{1.1}\text{Cu}_{26.4}\text{S}_{48.4}$, *tal* (Fig. 1c, $g \sim 1$, gray plates) and chalcopyrite (*cp*) $\text{Fe}_{24.1}\text{Ni}_{0.8}\text{Cu}_{26.1}\text{S}_{49.0}$ (Fig. 1c, $g \sim 1$, dark gray plates). A possible error in determining the exact composition of chalcopyrite is related to the small thickness of its plates ($\leq 1 \mu\text{m}$), which causes neighboring grains to occur in the electron beam of the analyzer. Both phases contain minor nickel.

Distribution of components in the sample. The data on the chemical analysis of primary phases (Table 1) were used to construct the distribution curves of components along the ingot up to $g = 0.96$ (Fig. 4) and their coefficients of distribution between solid phases and the melt were calculated (Fig. 5). The small value of the bottom Zone V results in big errors in the construction of dependence of melt composition of g . Therefore, we did not describe the crystallization process of phases in this zone.

It was mentioned above that monosulfide solid solution crystallizes in Zone I. During crystallization, Fe and Ni mainly pass into *mss* ($\kappa_{\text{Fe}} = 1.3\text{--}1.4$, $\kappa_{\text{Ni}} = 1.1\text{--}1.3$). Sulfur has a weak tendency to concentrate in a solid ingot ($\kappa_{\text{S}} \sim 1.06$), and Cu is intensively pushed into the melt ($\kappa_{\text{Cu}} = 0.25\text{--}0.28$). In Zone II, nonstoichiometric isocubanite *icb** crystallizes (Table 1). During its crystallization, sulfide melt becomes enriched in nickel ($\kappa_{\text{Ni}} = 0.53$) and copper ($\kappa_{\text{Cu}} =$

0.86). In spite of the fact that Zone III occupies a large part of the ingot, the composition of *iss*₁ formed from the melt changes slightly. The distribution coefficients of components are close to 1 (Fig. 5). In Zone IV, an intermediate solid solution also crystallizes but the composition of *iss*₂ differs significantly from *iss*₁. During crystallization of *iss*₂, the melt becomes enriched with Fe ($\kappa_{\text{Fe}} = 0.8\text{--}0.7$) and Ni ($\kappa_{\text{Ni}} = 0.8\text{--}0.6$), and solid phase, with Cu ($\kappa_{\text{Cu}} = 1.2\text{--}1.6$) and S ($\kappa_{\text{S}} \sim 1.1$).

Figure 5 shows the change in the distribution coefficients of components between the solid ingot and the melt during crystallization. The dependence of $\kappa(g)$ is described by a piecewise smooth curve, the discontinuities of which correspond to the transitions from one zone to the adjacent zone owing to the change in the phase composition of solid sample.

DISCUSSION OF RESULTS

Reactions of formation of solid phases from melt. The experimental melt composition belongs to the four-dimensional volume of primary crystallization of *mss* in the 4D-space of the phase diagram of the quaternary system Cu–Fe–Ni–S. Therefore, *mss* ($L \rightarrow mss$) is to crystallize in Zone I. However, the studied sample lacks a single-phase zone of *mss*, but contains a mixture of *mss* + *icb**. The appearance of *icb** can be related to the partial decay of Cu-

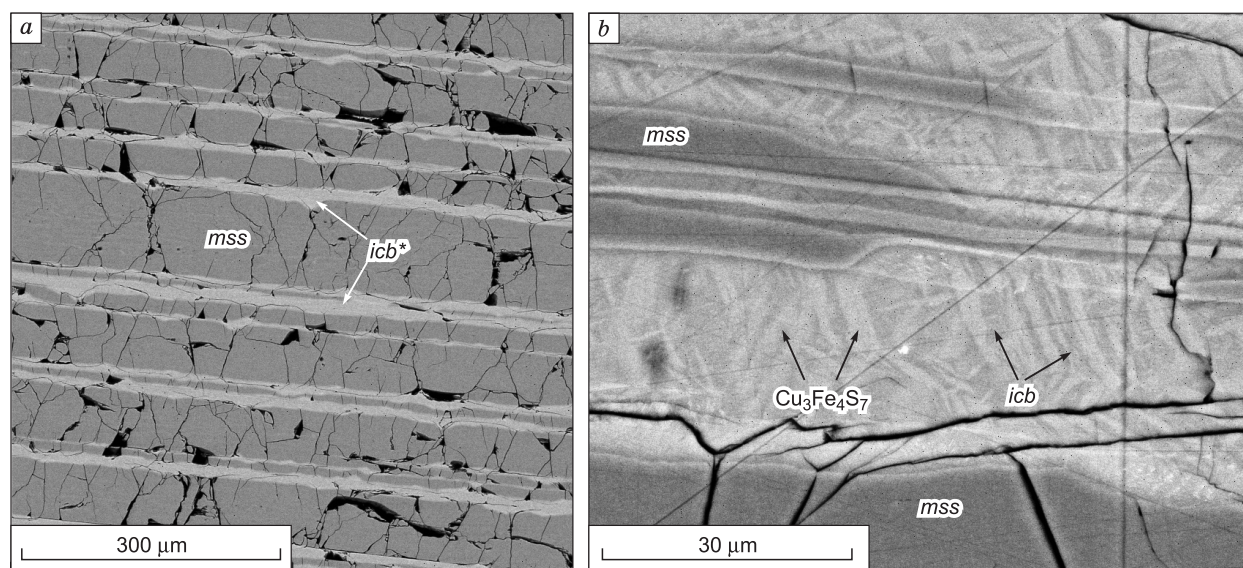


Fig. 2. Microstructure of zone I. *a*, Matrix of low-temperature monosulfide solid solution (*mss*) with lamellar inclusions the average composition of which corresponds to nonstoichiometric isocubanite ($\text{Cu}_{18.4\pm 0.3}\text{Fe}_{30.7\pm 0.3}\text{Ni}_{0.3\pm 0.05}\text{S}_{50.6\pm 0.1}$, *icb**); *b*, *icb** lamellas are formed from stoichiometric isocubanite (CuFe_2S_3 , *icb*) and phases, the composition of which is close to $\text{Cu}_3\text{Fe}_4\text{S}_7$ described in (Schlegel and Schüller, 1952). Black is pores and cracks in the sample. Photomicrographs were obtained in back-scattered electrons.

doped *mss*, and the excess copper is separated as isocubanite. Then the trajectory of melt composition passes through the small Zone II of primary crystallization of *icb**. The transition from Zone I to Zone II can be interpreted as the proof of phase reaction: $L + mss \rightarrow icb^*$. In accordance with the above-mentioned interpretation, a single solid phase of *iss*₁ crystallizes in Zone III. In the transition area between Zone II and Zone III a peritectic reaction: $L + icb^* \rightarrow iss_1$ must take place. In Zone IV, a discontinuous solid solution also crystallizes. At the boundary of Zones III and IV, the composition of solid solution changes abruptly. The struc-

ture of solid solution in this zone has not been determined yet. We assume that these phases can have a similar structure and the abrupt change in the composition can be related to the separation of *iss* into two phases: *iss*₁ and *iss*₂. In this case, peritectic reaction $L + iss_1 \rightarrow iss_2$ must proceed at the boundary between the zones. To correctly determine the possibility of the existence of two phases of *iss* on the phase diagram, it is necessary to carry out additional structural studies using *in situ* methods. The primary phases crystallized in Zone V decompose completely into secondary phases. Therefore, it is impossible to describe crystallization processes only on the basis of chemical analysis.

The complexity of phase relations in the basic system Fe–Cu–Ni–S affects the sequence of separation of minerals, whose compositions are similar to an intermediate solid solution (Spiridonov and Gritsenko, 2009; Spiridonov, 2010). It is worth noting that the compositions of some minerals are identical or differ slightly, so this requires a more thorough study of the change in phase and chemical composition of samples during crystallization of sulfide melt, in particular, using *in situ* researches.

Crystallization paths. To understand the features of fractionation of components, Fig. 6 illustrates the projections of trajectories of melt and solid phases on the (Me/ΣMe)–S plane during the formation of zones I–IV. The melt composition during the formation of different zones changes along the segments AB (Zone I), BC (II), CD (III), DE (IV) in the direction indicated by arrows. The compositions of solid phases change along segments FG (*mss*), H (*icb**), IJ (*iss*₁) and KM (*iss*₂). The monosulfide solid solution *mss* becomes enriched with copper and nickel and depleted in iron and sulfur.

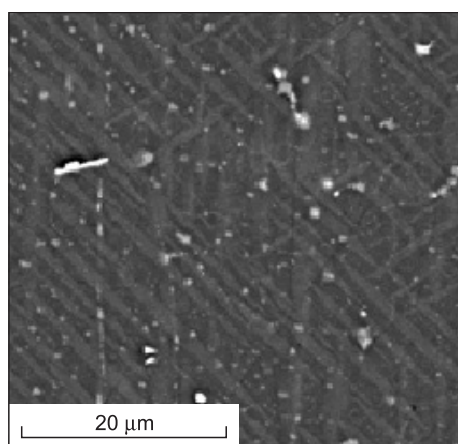


Fig. 3. Microstructure of the sample from zone II. Gray lamellas are isocubanite *icb* (CuFe_2S_3), dark gray lamellas are intermediate solid solution *iss* ($\sim\text{Cu}_2\text{Fe}_3\text{S}_5$), small light gray grains are, probably, pentlandite ($(\text{Fe},\text{Ni})_{9\pm 1}\text{S}_{8\pm 1}$). White inclusions are impurity phases containing platinumoids which are beyond the scope of this work. Photomicrograph was made in back-scattered electrons.

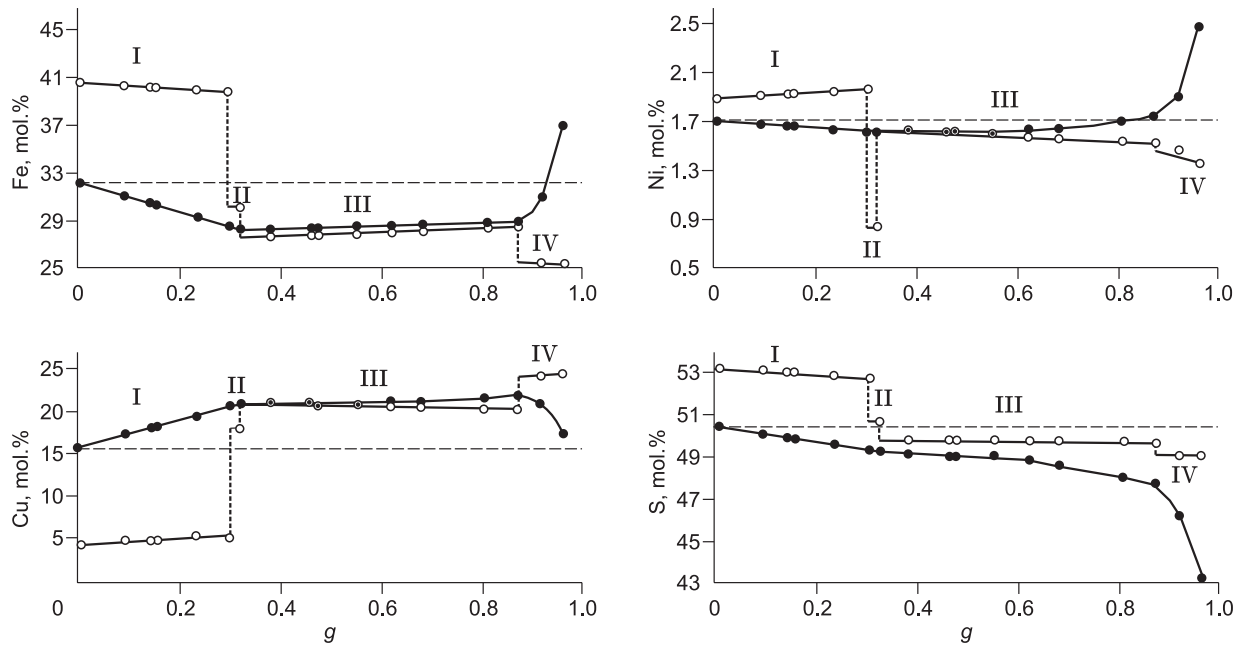


Fig. 4. Distribution curves of Fe, Ni, Cu and S in the ingot after directed crystallization. Open circles are average concentrations of components in the solid ingot, closed circles are average concentrations in the melt. Dashed horizontal line shows the component concentration in the initial melt. Dashed vertical lines divide the zones. Segments I–IV correspond to the crystallization of various zones. Zone V is not shown.

Each *mss* composition corresponds to equilibrium melt composition. The compositions of these phases are connected by conodes, and their association forms a fan of conodes. Owing to the small length of Zone II, the composition of isocubanite *icb** changes slightly and the fan degenerates into a straight line. The composition of the intermediate solid solution *iss₁* during crystallization also changes insignificantly

while the concentration of nickel, copper and sulfur in it decreases, and that of iron, increases. The melt becomes strongly depleted in sulfur and relatively poorly enriched in copper and nickel. Sulfur concentration in the intermediate solid solution *iss₂* is virtually constant, this phase becomes poor in nickel and weakly enriched in copper. The composition of the melt during crystallization

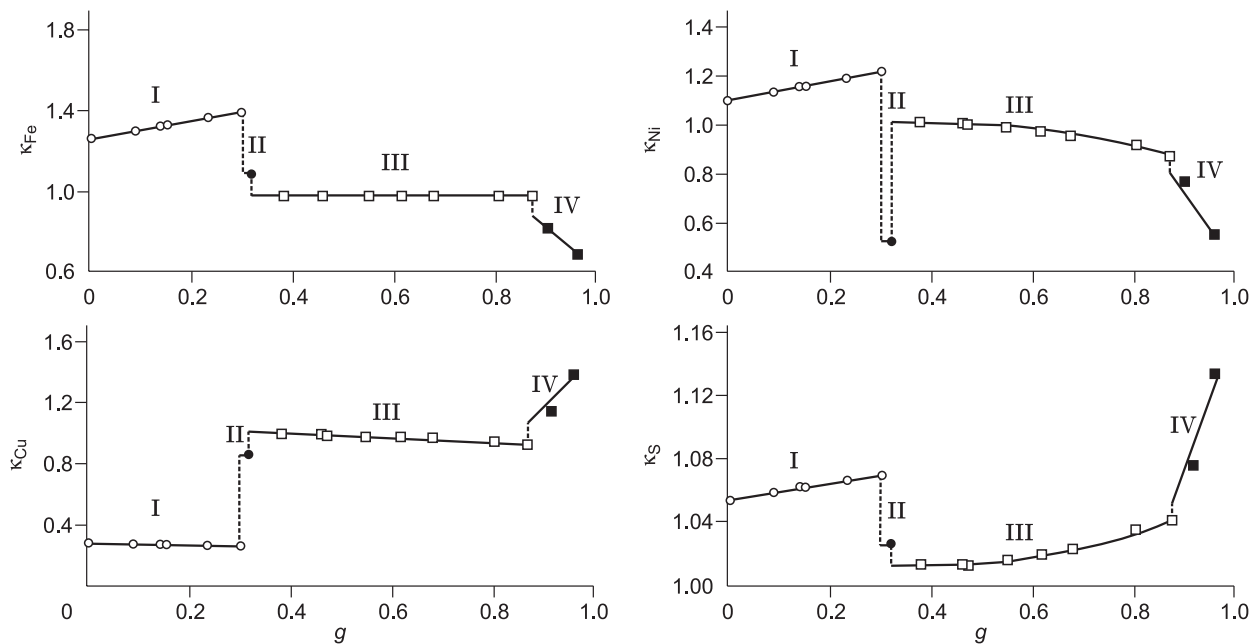


Fig. 5. Change in the distribution coefficients of Fe, Ni, Cu and S during crystallization. Open circles are $\kappa(mss/L)$, closed circles are $\kappa(icb^*/L)$, open squares are $\kappa(iss_1/L)$, closed squares are $\kappa(iss_2/L)$. Dashed vertical lines divide the zones. Zone V is not shown.

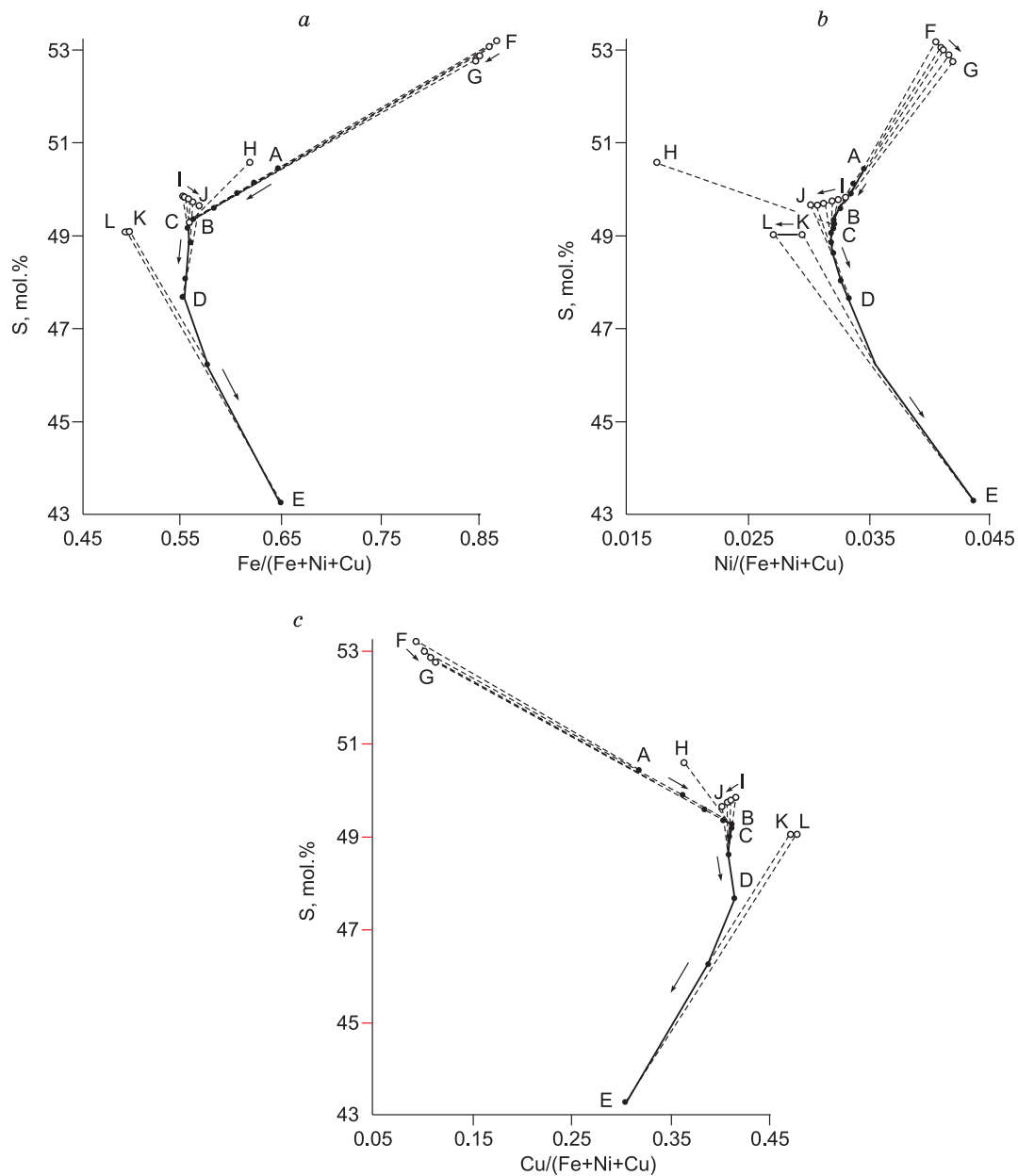


Fig. 6. Projections of the curves of melt, *mss*, *icb**, *iss₁*, *iss₂* composition and “fans” of conodes onto the face Fe/(Fe + Ni + Cu)–S (a), Ni/(Fe + Ni + Cu)–S (b) and Cu/(Fe + Ni + Cu)–S (c) during directional crystallization of the sample. A is the composition of the initial sample; AB, BC, CD and DE are crystallization paths of the melt during the formation of *mss*, *icb**, *iss₁* and *iss₂*, respectively; FG, H, IJ and KL are the compositions of *mss*, *icb**, *iss₁* and *iss₂*. The arrows show the direction of changes in the composition of melt and solid phases during crystallization, dashed lines show the projection of conodes.

changes drastically: it becomes depleted in copper and sulfur and enriched in iron and nickel.

In Fig. 6, the trajectory of the melt’s composition is a piecewise smooth line that successively passes through different parts of liquidus hypersurface. The points of the solid phase compositions belong to spatially isolated parts of solidus hypersurface. The figure illustrates that *mss*, *iss₁* and *iss₂* phase are solid solutions, and isocubanite is an approximately stoichiometric compound. The phase diagram clearly dis-

plays how transition between the crystallization fields of *iss₁* and *iss₂* takes place.

Thus, the possibility of using directed crystallization of melt for obtaining new unique system data on the solid-liquid diagram of a multicomponent system has been confirmed once again. It was shown that the Cu–Fe–Ni–S system has a two-phase region *L* + *icb**. It was revealed earlier that such region exists in the ternary Cu–Fe–S system (Kosyakov and Sinyakova, 2017b). We showed the existence of two solid

solutions designated as iss_1 and iss_2 . These solid solutions were for the first time mentioned in (Fleet and Pan, 1994). Crystallization of phases icb^* , iss_1 and iss_2 from the melt was found to have a peritectic character.

Subsolidus phase processes. Interpretation of the experimental results on the directed crystallization is complicated by the subsolidus phase reactions that proceed during cooling of the sample. In fact, the system under study contains some high-temperature phases, which decompose completely or partially. In addition, when the temperature of solid solutions decreases, the homogenization region typically reduces too. This leads to the formation of inclusions of decay products of the primary solid solutions.

In Zone I, the sample is a matrix of iron-rich mss with inclusions of nonstoichiometric isocubanite. During the separation of isocubanite, the mss matrix becomes depleted in copper. This implies that the solubility of copper in mss reduces with decreasing temperature. The reduction of the size of the homogenization region leads to the transition of the figurative point of sample composition from the single-phase region mss to the two-phase region $mss + icb^*$. With a further decrease in temperature, icb^* decomposes into a mixture of stoichiometric icb ($CuFe_2S_3$) and compounds with a composition similar to $Cu_3Fe_4S_7$. These phases dissolve a small amount of nickel (0.2–0.4 mol.%). The presence of such segregations indicates the existence of a conode on the subsolidus diagram of the Cu–Fe–Ni–S system near the bounding ternary Cu–Fe–S system. The conode links phases $CuFe_2S_3$ and $Cu_3Fe_4S_7$. It is worth noting that according to data from (Merwin and Lombard, 1937), $CuFe_2S_3$ and compounds of composition from $Cu_3Fe_4S_7$ to $Cu_2Fe_4S_7$ are stable in the Fe-rich region of the Cu–Fe–S system.

The microstructure of Zone II consists of lamellar intergrowths of stoichiometric isocubanite, iss of composition $\sim Cu_2Fe_3S_5$ and isometric micron inclusions of pentlandite. Probably, the formation of lamellas is the result of a decay reaction like $icb^* = CuFe_2S_3 + iss$ ($\sim Cu_2Fe_3S_5$), and separation of pentlandite is, most likely, a lower temperature process of a decrease in the solubility of nickel in icb upon its cooling.

The microstructure of Zone III corresponds to the decomposition of iss_1 into a mixture of nonidentified decay products. The microstructure of Zone IV is a mixture of oriented lamellas of chalcopyrite cp and putoranite put . Most likely, it results from a complete decomposition of an intermediate solid solution by the reaction $iss_2 \rightarrow cp + put$. Zone V is a mixture of tabular segregations of talnakhite, chalcopyrite and bornite, which was probably formed by the reaction $iss_3 \rightarrow tal + cp + bn$.

Thus, the studied region of the subsolidus diagram of the system Cu–Fe–Ni–S can contain two-phase regions $mss + icb^*$, $icb + Cu_3Fe_4S_7$, $icb + iss$ ($\sim Cu_2Fe_3S_5$), $icb + pn$, $cp + put$, and the three-phase region $tal + cp + bn$.

On the other hand, the study of the structure and composition of directly crystallized samples allowed us to obtain use-

ful information on the regularities of subsolidus processes, which can be used to predict a new type of complex zonality of natural mineral associations in copper-rich sulfide ores.

One should not expect an absolute coincidence of the results of experimental modeling for the sequence of formation of minerals associations in the directly crystallized sample and in copper-rich zoned ore bodies. Firstly, real melts contain more components than the experimental sample. The addition of a new component can occasionally lead to a considerable change in the sequence of separation of phases. Secondly, a multicomponent system can contain phases that are absent in the system with fewer components, which can result in a more complicated zonality compared to a model system with fewer components. Thirdly, the sequence of separation of phases in a particular chemical system might be very sensitive to the composition of the initial melt (for example (Kosyakov et al., 2012)). Fourthly, in fact the interpretation used here refers to a conservative system in which the melt and solid phases do not interact with the environment. In a real geochemical system, the conservation condition may not be realized. In this case, new phases can appear in the system and the character of zonality can change. Fifthly, natural processes of crystallization fractionation may occur in nonstrictly conservative systems.

In this work, we modeled a new possible variant of complex zonality of copper-nickel ore bodies. It is worth noting that the general regularities of distribution of the main components in the sample are in qualitative agreement with the generalized results of study of massive ore bodies from the Noril'sk–Tanah deposits reported in (Genkin et al., 1981; Distler, 1994; Distler et al., 1988; Andretti, 2004; Sluzhenikin, 2011; Sluzhenikin and Mokhov, 2015; Duran et al., 2017). For a reliable description of the relationship between the composition of parent sulfide liquids and types of zonality of ore bodies and for substantiation of physicochemical causes for the variety of types of primary zonality, it is necessary to carry out a complete research of the structure of a continuous hypersurface of the liquidus and piecewise hypersurface of a solidus in the important fragments of the phase diagram of the Cu–Fe–Ni–S system. Hence, it is necessary to conduct a directed crystallization of melts in all the fields of primary crystallization of minerals in the concentration tetrahedron and to supplement these researches by in situ studies of sequential appearance and disappearance of phases on heating and cooling of samples.

CONCLUSIONS

(1) The possibility of the presence of a previously undescribed type of zonality is shown in a laboratory experiment on the fractionation crystallization of copper-rich and nickel-poor sulfide Cu–Fe–Ni melt.

(2) New data on the location of the melt crystallization paths and solid phases on liquidus and solidus surfaces, on

the position of the fans of conodes in a concentration tetrahedron, and on the existence of crystallization fields of $L + mss$, $L + icb^*$, $L + iss_1$, $L + iss_2$ were obtained on the fragment of the phase diagram of the Cu–Fe–Ni–S system near the Cu–Fe–S boundary system. In addition, the values of the distribution coefficients of the components along the crystallization path were calculated and the equation of phase reactions were determined when the trajectories moved from one zone to the neighboring zone.

(3) Data on the probable phase associations and some phase reactions in the subsolidus region of phase diagram are obtained.

The study was carried out within the framework of state assignments (projects II.1.64.4 and 0330-2016-0001) and with partial financial support from the integrated program of basic scientific research of the SB RAS II.1. No. 303.

REFERENCES

- Cabri, L.J., 1973. New data on phase relations in the Cu–Fe–S system. *Econ. Geol.* 68, 443–454.
- Craig, J.R., Kullerud, G., 1969. Phase relations in the Cu–Fe–Ni–S system and their application to magmatic ore deposits, in: Wilson, H.D.B. (Ed.), *Magmatic Ore Deposits. Soc. Explor. Geophys., Geophys. Monogr. Ser., Vol. 4*, pp. 344–358.
- Czamanske, G.K., Kunilov, V.E., Zientek, M.L., Cabri, L.J., Likchachev, A.P., Calk, L.C., Oscarson, R., 1992. A proton microprobe study of magmatic sulfide ores from the Noril'sk-Talnakh district, Siberia. *Can. Mineral.* 30 (2), 249–287.
- Distler, V.V., 1994. Platinum mineralization of the Noril'sk deposits, in: *Geology and Genesis of Deposits of Platinum Group Metals [in Russian]*. Nauka, Moscow.
- Distler, V.V., Grokhovskaya, T.L., Evstigneeva, T.L., Sluzhenkin, S.F., Filimonova, A.A., Dyuzhikov, O.A., Laputina, I.P., 1988. *Petrology of Sulfide Magmatic Mineralization [in Russian]*. Nauka, Moscow.
- Duran, C.J., Barnes, S.-J., Pleše, P., Prašek, M.K., Zientek, M.L., Pagé, P., 2017. Fractional crystallization-induced variations in sulfides from the Noril'sk-Talnakh mining district (polar Siberia, Russia). *Ore Geol. Rev.* 90, 326–351.
- Ebel, D.S., Naldrett, A.J., 1997. Crystallization of sulfide liquids and the interpretation of ore composition. *Can. J. Earth Sci.* 34 (4), 352–365.
- Fleet, M.E., Pan, Y., 1994. Fractional crystallization of anhydrous sulfide liquid in the system Fe–Ni–Cu–S, with application to magmatic sulfide deposits. *Geochim. Cosmochim. Acta* 58 (16), 3369–3377.
- Genkin, A.D., Distler, V.V., Gladyshev, G.D., Filimonova, A.A., Evstigneeva, T.L., Kovalenker, V.A., Laputina, I.P., Smirnov, A.V., Grokhovskaya, T.L., 1981. *Sulfide Copper-Nickel Ores of the Noril'sk Deposits [in Russian]*. Nauka, Moscow.
- Kosyakov, V.I., Sinyakova, E.F., 2005. Directional crystallization of Fe–Ni sulfide melts within the crystallization field of monosulfide solid solution. *Geochem. Int.* 43 (4), 372–385.
- Kosyakov, V.I., Sinyakova, E.F., 2010. Primary, secondary, and admixture zonation of copper-nickel ores during fractional crystallization of sulfide melts. *Dokl. Earth Sci.* 432 (6), 829–834.
- Kosyakov, V.I., Sinyakova, E.F., 2012. Physicochemical prerequisites for the formation of primary orebody zoning at copper-nickel sulfide deposits (by the example of the systems Fe–Ni–S and Cu–Ni–S). *Russian Geology and Geophysics (Geologiya i Geofizika)* 53 (9), 861–882 (1126–1153).
- Kosyakov, V.I., Sinyakova, E.F., 2014. Melt crystallization of $CuFe_2S_3$ in the Cu–Fe–S system. *J. Therm. Anal. Calorim.* 115 (1), 511–516.
- Kosyakov, V.I., Sinyakova, E.F., 2017a. Experimental modeling of pentlandite-bornite ore formation. *Russian Geology and Geophysics (Geologiya i Geofizika)* 58 (10), 1211–1221 (1528–1541).
- Kosyakov, V.I., Sinyakova, E.F., 2017b. Study of crystallization of nonstoichiometric isocubanite $Cu_{1.1}Fe_{2.0}S_{3.0}$ from melt in the system Cu–Fe–S. *J. Therm. Anal. Calorim.* 129 (2), 623–628.
- Kosyakov, V.I., Sinyakova, E.F., Distler, V.V., 2012. Experimental simulation of phase relationships and zoning of magmatic copper-nickel sulfide ores, Russia. *Geologiya Rudnykh Mestorozhdeniy* 54 (3), 221–252.
- Lavrent'ev, Yu.G., Karmanov, N.S., Usova, L.V., 2015. Electron probe microanalysis of minerals: Microanalyzer or scanning electron microscope? *Russian Geology and Geophysics (Geologiya i Geofizika)* 56 (8), 1154–1161 (1473–1482).
- Merwin, H.E., Lombard, R.H., 1937. The system Cu–Fe–S. *Econ. Geol.* 32, 203–284.
- Naldrett, A.J., 2004. *Magmatic Sulfide Deposits. Geology, Geochemistry and Exploration*. Springer-Verlag, Heidelberg.
- Naldrett, A.J., 2010. From the mantle to the bank: the life of a Ni–Cu–(PGE) sulfide deposit. *S. Afr. J. Geol.* 113 (1), 1–32.
- Schlegel, H., Schüller, A., 1952. Das Zustandebild Kupfer-Eisen-Schwefel. *Z. Metallkunde* 43 (12), 421–442.
- Sinyakova, E.F., Kosyakov, V.I., 2009. Experimental modeling of zonation of copper-rich sulfide ores in copper-nickel deposits. *Dokl. Earth Sci.* 427 (1), 787–792.
- Sinyakova, E.F., Kosyakov, V.I., 2012. The behavior of noble-metal admixtures during fractional crystallization of As- and Co-containing Cu–Fe–Ni sulfide melts. *Russian Geology and Geophysics (Geologiya i Geofizika)* 53 (10), 1055–1076 (1374–1400).
- Sinyakova, E., Kosyakov, V., Distler, V., Karmanov, N., 2016. Behavior of Pt, Pd, and Au during crystallization of Cu-rich magmatic sulfide minerals. *Can. Mineral.* 54 (2), 491–509.
- Sluzhenkin, S.F., 2011. Platinum-copper-nickel and platinum ores of Noril'sk Region and their ore mineralization. *Russ. J. Gen. Chem.* 81 (6), 1288–1301.
- Sluzhenkin, S., Mokhov, A., 2015. Gold and silver in PGE–Cu–Ni and PGE ores of the Noril'sk deposits, Russia. *Miner. Deposita* 50 (4), 465–492.
- Spiridonov, E.M., 2010. Ore-magmatic systems of the Noril'sk ore field. *Russian Geology and Geophysics (Geologiya i Geofizika)* 51 (9), 1059–1077 (1356–1378).
- Spiridonov, E.M., Gritsenko, Yu.D., 2009. Epigenetic Low-Grade Metamorphism and Co–Ni–Sb–As Mineralization in the Noril'sk Ore Field [in Russian]. Nauchnyi Mir, Moscow.